INTERNATIONAL JOURNAL FOR NUMERICAL METHODS IN BIOMEDICAL ENGINEERING
*Int. J. Numer. Meth. Biomed. Engng.* (2015); e02716
Published online 28 April 2015 in Wiley Online Library (wileyonlinelibrary.com). DOI: 10.1002/cnm.2716

# Finite element simulation of the insertion of guidewires during an EVAR procedure: example of a complex patient case, a first step toward patient-specific parameterized models

Juliette Gindre[1,2,3,4,5,*,†], Aline Bel-Brunon[1,2], Adrien Kaladji[3,4,6], Aurélien Duménil[3,4,7], Michel Rochette[5], Antoine Lucas[3,4,6], Pascal Haigron[3,4] and Alain Combescure[1,2]

[1]*Université de Lyon, Lyon F-69000, France*
[2]*LaMCoS CNRS UMR5259, INSA-Lyon, Villeurbanne F-69621, France*
[3]*INSERM U1099, Rennes F-35000, France*
[4]*LTSI, Université de Rennes 1, Rennes F-35000, France*
[5]*ANSYS, Villeurbanne F-69100, France*
[6]*Department of Vascular Surgery, CHU Rennes, Rennes F-35000, France*
[7]*THERENVA, Rennes F-35000, France*

SUMMARY

Deformations of the vascular structure due to the insertion of tools during endovascular treatment of aneurysms of the abdominal aorta, unless properly anticipated during the preoperative planning phase, may be the source of intraoperative or postoperative complications. We propose here an explicit finite element simulation method which enables one to predict such deformations. This method is based on a mechanical model of the vascular structure which takes into account the nonlinear behavior of the arterial wall, the prestressing effect induced by the blood pressure and the mechanical support of the surrounding organs and structures. An analysis of the model sensitivity to the parameters used to represent this environment is done. This allows determining the parameters that have the largest influence on the quality of the prediction and also provides realistic values for each of them as no experimental data are available in the literature. Moreover, for the first time, the results are compared with 3D intraoperative data. This is done for a patient-specific case with a complex anatomy in order to assess the feasibility of the method. Finally, the predictive capability of the simulation is evaluated on a group of nine patients. The error between the final simulated and intraoperatively measured tool positions was 2.1 mm after the calibration phase on one patient. It results in a $4.6 \pm 2.5$ mm in average error for the blind evaluation on nine patients. Copyright © 2015 John Wiley & Sons, Ltd.

Received 17 November 2014; Accepted 20 March 2015

KEY WORDS: Endovascular; Abdominal aortic aneurysm; patient-specific; surrounding organs support; 3D intraoperative data

## 1. INTRODUCTION

Endovascular aneurysm repair (EVAR) is a commonly used mini-invasive technique which has gained increasing popularity over the last 10 years. It relies on the exclusion of the aneurysm sac by means of the femoral introduction of one or more stent grafts and their deployment inside the aneurysm. During the procedure, several tools of varying stiffness are introduced to enable the delivery of the stent graft to its deployment site: first, highly flexible guidewires and catheters which adapt to the arterial lumen, then very stiff guidewires whose purpose is to facilitate the passage of and provide support for the stent graft introducer, in particular by straightening the often tortuous iliac arteries. During this process, the vascular structure undergoes major deformations [1]. Usually,

*Correspondence to: Gindre Juliette, LaMCoS CNRS UMR5259. INSA-Lyon, Villeurbanne F-69621, France.
†E-mail: juliette.gindre@ansys.com

 

these have no consequence on the smooth progress of the procedure. However, in some instances, particularly when the patient presents an unfavorable anatomical profile (major tortuousness or angulation, deep calcification, and long length of the common and external iliac arteries), the deformation caused by the insertion of stiff guidewires can have major consequences. Straightening tortuous arteries may lead to shrinkage of the arterial segments compared with the preoperative anatomy, thus calling into question the initial sizing of the stent grafts. It can also induce major movements of anatomical markers such as the ostia of the digestive arteries, leading, in the most critical cases, to a risk of covering a secondary artery [2]. Conversely, in some cases, the tools are incapable of straightening excessively calcified and tortuous arteries, thus precluding the delivery of the stent graft, which usually leads to an amendment of the procedure or to its cancelation [3].

Arterial deformations caused by the endovascular equipment during surgery depend on multiple factors, such as the morphology of the arteries, the state and degree of calcification of the arterial wall, and also the types of devices used. Today, their prediction relies mainly on the surgeon's experience. Numerical simulation appears to be an appropriate tool to anticipate the complications mentioned earlier. Its use in the preoperative phase could give the practitioner more objective and more useful indicators when planning the procedure: guiding the surgical act and making it safer using such an approach would potentially reduce the risks of intraoperative and postoperative complications.

In recent years, research on the use of finite element simulations in the vascular domain has intensified. Many studies have focused on the use of finite elements for determining the risk of aneurysm rupture through the calculation of parietal stresses induced by arterial pressure [4–6]. More recently, some studies have been published on the deployment of abdominal or thoracic stent grafts over patient-specific geometries [7, 8]. Finally, as far as we know, only three studies exist in the literature concerning the finite element simulation of the deformation of the vascular structure due to the insertion of endovascular guidewires. Gupta *et al.* [9] compared two implicit and explicit finite element calculation methods for the simulation of the progressive insertion of an endovascular guidewire into an iliac artery; however, the method was tested on only one anatomy, and no validation against intraoperative data was proposed. Two studies addressed an implicit finite element calculation method for the deformation caused by the insertion of an 'extra-stiff' guidewires into the vascular structure during an EVAR procedure [10, 11]. However, the published results were compared with only 2D intraoperative data, and the implicit method used showed convergence difficulties when facing tortuous anatomies. Finally, Mouktadiri *et al.* [12] showed the feasibility of the use of the explicit finite element method in the simulation of the insertion of endovascular devices; however, no extra-stiff guidewires were modeled and no quantitative information regarding comparisons with intraoperative data was presented.

Here, we present the development of a method for the simulation of the deformation of the vascular structure due to the insertion of extra-stiff guidewires during an EVAR procedure using an explicit finite element software. The simulation is presented on a patient-specific case involving a complex anatomy in order to prove the feasibility of the method, and the results are compared with 3D imaging data acquired during the surgical procedure. The support provided by surrounding organs and bones structures is taken into account in a more realistic way than what was proposed in previous publications [11, 12]. As very few clinical or experimental data are available concerning this particular aspect, we carried out a sensitivity study to understand the effect of the parameters introduced to model the external support. Finally, a blind evaluation was conducted on a group of nine patients to evaluate the predictive capability of the simulation.

## 2. MATERIALS AND METHODS

### *2.1. General description of the workflow*

Three 3D data acquisitions of the patient's vascular structure were performed during this research. A preoperative computed tomography (CT) scan was used to build the numerical model for the simulation; an intraoperative acquisition, denoted 'undeformed CBCT', prior to deformation by the tools led to the registration of the intraoperative data in the preoperative coordinate system; finally,



DOI: 10.1002/cnm

an intraoperative acquisition after insertion of the deforming tools, denoted 'deformed CBCT', once registered in the preoperative coordinate system, enabled us to compare the results of the simulation with the intraoperative reality. The following diagram (Figure 1) summarizes the different acquisitions and their use in the creation and validation of the numerical model.

### 2.2. *Considered patient case and available preoperative data*

The study protocol was approved by the institutional review board. Patient informed consent was obtained for being registered anonymously in the database. The case study we focused on was that of a 63-year-old patient who underwent an EVAR procedure in the vascular surgery department at the University Hospital of Rennes, France. The available preoperative data were a CT angiogram composed of 1117 slices (thickness 0.75 mm, pixel size 0.75 mm × 0.75 mm). According to common clinical practice, the data were first processed through the ENDOSIZE® commercial sizing software (Therenva, Rennes, France) in order to extract a segmentation of the vascular lumen, the centerlines of the blood vessels, and density values of the vascular wall for tissue classification purposes (healthy wall, calcifications). Then, an analytical geometry of the lumen and a triangular surface mesh (Figure 2) were obtained using a method described in a previous work [10]. Finally, we extracted additional data which were necessary to build the biomechanical model, such as specific anatomic points (ostia of the internal iliac arteries) and a map of the distances from the vascular wall to the spine.

### 2.3. *The numerical model*

#### 2.3.1. *Modeling of the vascular structure.*

a. **Description of the geometry**

The vascular geometry represented in the simulations corresponds to an aorto-iliac structure consisting of the abdominal aorta and the common and external iliac arteries as far as the femoral bifurcations. The collateral arteries were not represented in the geometry, but their mechanical effect was partially taken into account by suitable boundary conditions, as described in Paragraph 2.3.1.c.

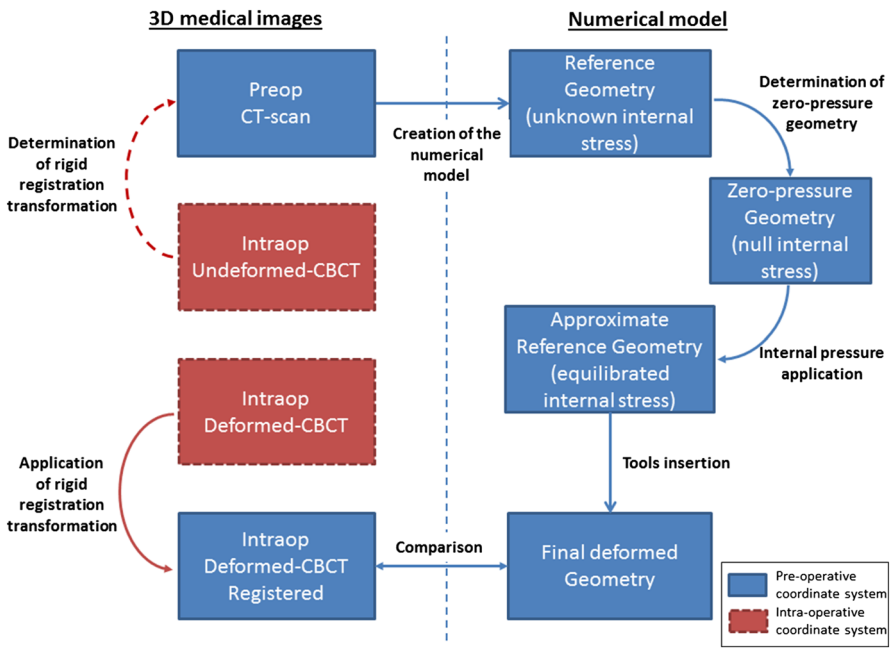


Figure 1. Illustration scheme of the general workflow. CT, computed tomography; CBCT, cone-beam CT.



DOI: 10.1002/cnm

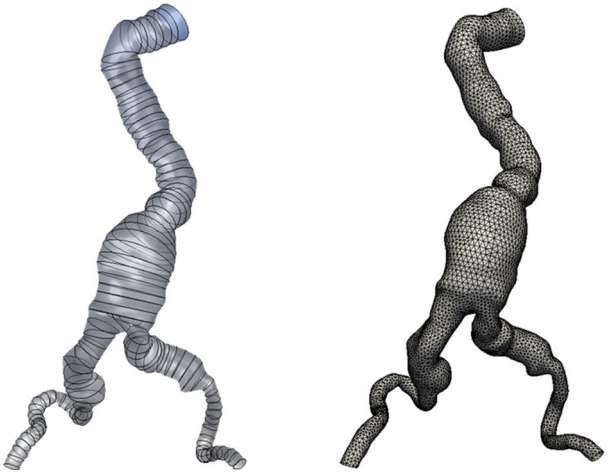

Figure 2. Surfacic geometry and finite element mesh of the vascular structure.

The represented surface corresponds to the internal surface of the arterial lumen. The intraluminal thrombus was not represented in the model.

b. **Modeling of the mechanical behavior of the vascular wall**

The vascular structure was meshed using 8796 nodes and 17,532 Discrete Kirchhoff Triangular (DKT) triangular shell elements, whose characteristic size varied between about 1 and 3 mm. Although these elements can behave over-stiffly in membrane because strain is uniform in each of them, we chose them for their meshing ability. We ran a mesh convergence analysis (Section 3.1.2), which shows that the element size in the model is small enough to overcome the poor discretization of membrane strains in DKT. The mesh elements were given a constant thickness of 1.5 mm for the aorta and of 1.2 mm for the iliac arteries, in accordance with values reported in the literature [13–15]. In a first approach, although it is now known that a healthy aneurysmal aortic wall has anisotropic behavior, we chose to model the behavior of the arterial wall using the polynomial, nonlinear, and isotropic hyperelastic potential defined by Equation (1):

$$W = C_{10}(I_1 - 3) + C_{20}(I_1 - 3)^2 \tag{1}$$

Simulations of biaxial tests were carried out using this model and compared with the experimental results given by Vande Geest *et al.* [14] in order to determine realistic values for parameters $C_{10}$ and $C_{20}$. The resulting values used in the simulations are $C_{10} = 0.005$ MPa and $C_{20} = 0.2$ MPa.

It is also commonly accepted that the state of calcification of the iliac arteries can influence the deformations created by the endovascular devices [3, 16]. Therefore, two different types of behavior, corresponding, respectively, to a healthy arterial tissue and to a calcified plaque, were assigned to the elements depending on the corresponding voxel density in the CT scan, as described in [11]. The calcified elements were all assigned the same linear elastic properties (Young's modulus $E = 40$ MPa, Poisson's ratio $\upsilon = 0.4$) corresponding to highly calcified tissue as reported in [17]. Let us note, however, that the patient case we studied presented only a small number of calcifications, so their influence on the global behavior of the model was limited.

c. **Loading and boundary conditions**

### *2.4. Modeling of the external environment mechanical support*

The deformations undergone by the vascular structure due to the endovascular devices are very dependent on its anatomy and its relationship with the surrounding organs and tissues. Therefore, it is crucial for the reliability of the simulations to take into account this environment properly in the boundary conditions of the model. In the literature, only a handful of authors discuss modeling



DOI: 10.1002/cnm

methods for the mechanical support due to the external environment of the vascular structure. Liu *et al.* [18] and Zhang *et al.* [19] showed that this support can be partially taken into account by the application of a uniform external pressure called the 'effective perivascular pressure'. In the context of fluid–structure simulations, Moireau *et al.* [20] modeled the support of the rachis and perivascular tissues of the thoracic aorta using viscoelastic boundary conditions over the wall surface, leading to a relation among the stresses, displacements, and velocities in the wall.

Thus, the external loads that were applied to model the effect of the external environment of the vascular structure on the wall were composed of three parts: an elastic spring term, which depends on the displacement of the wall; a viscosity term, which depends on its velocity; and a constant internal pressure term. Therefore, at every node of the artery mesh, the external load due to the external environment can be expressed by Equation (2):

$$\overrightarrow{f}_{\text{ext}} = \overrightarrow{t}_{\text{ext}}.dS = \left(-k\overrightarrow{u} - c\overrightarrow{v} + p\overrightarrow{n}\right).dS \tag{2}$$

where $\overrightarrow{u}$ is the displacement of the considered mesh node, $\overrightarrow{v}$ the velocity of the node, $\overrightarrow{n}$ the vector normal to the surface at this node, $k$ the surfacic stiffness coefficient of the support, $c$ the surfacic viscosity coefficient of the support, $p$ the external pressure, $\overrightarrow{f}_{\text{ext}}$ the resultant external force vector, and $dS$ the elementary surface.

*2.4.1. Elastic support.* The elastic stiffness $k$, which represents the support from the surrounding organs and tissues (organs, *vena cava* and its branches, collateral arteries, and conjunctive tissues), is a function of the vascular segments considered as follows: healthy aorta ($k_1$), aneurysmal aorta ($k_3$), common iliac arteries ($k_5$), and external iliac arteries ($k_7$). In addition, along the segments corresponding to the aorta and the common iliac arteries, a supplementary stiffness $k_{\text{bones}}$, which decreases with the distance $d$ to the rachis, was used to model the strong link between the posterior face in contact with the rachis and the vertebral arteries created by the aortic fibrous bed. Let $k_{\max}$ denote the value of maximum stiffness of the bones support when $d = 0$ mm and $d_{\max}$ denoting the distance of effect of the bones support beyond which bones support is considered to be zero. Then the law defining the additional bones support is given by Equation (3):

$$\begin{aligned} k_{\text{bones}} &= k_{\max}(1 - d/d_{\max})^2 \quad \text{if} \quad d \le d_{\max} \\ k_{\text{bones}} &= 0 \quad \text{if} \quad d > d_{\max} \end{aligned} \tag{3}$$

Finally, an elastic stiffness $k_{\text{iliac}}$ was added locally at the beginning of the internal iliac arteries in order to represent the limited mobility of these points. As no experimental data are available concerning support parameters, values for $k_{\max}$ and $k_{\text{iliac}}$ were empirically determined and set to 0.005 MPa/mm which corresponds to a condition of very stiff support at a zero distance from the rachis and at the location of internal iliac arteries's ostia. On the other hand, the sensitivity of the model with regard to the parameters $k_1$, $k_3$, $k_5$, $k_7$, and $d_{\max}$ is studied in order to assess their effect on the simulation result and determine realistic values for each of them.

Figure 3. summarizes the stiffness distribution of the elastic support over the vascular structure.

*2.4.2. Viscosity.* The viscosity term $c$ represents the set of natural damping forces due to the tissues and biological fluids in contact with the vascular structure. This term was chosen to be uniform throughout the vascular structure. The choice of its numerical value is explained in Paragraph 2.3.3.3.

*2.4.3. External pressure.* The hydrostatic term $p$ accounts for the effect of all the fluids and soft tissues of the retroperitoneal cavity, which exert a relatively small (yet non-negligible) pressure, as reported in [18]. This term was chosen to be equal to 30 mmHg over the whole surface of the vascular structure and was simply subtracted from the internal pressure described in the following paragraph.

The relatively stationary proximal and distal extremities were modeled by a zero-displacement condition over the three outer borders of the mesh.



DOI: 10.1002/cnm

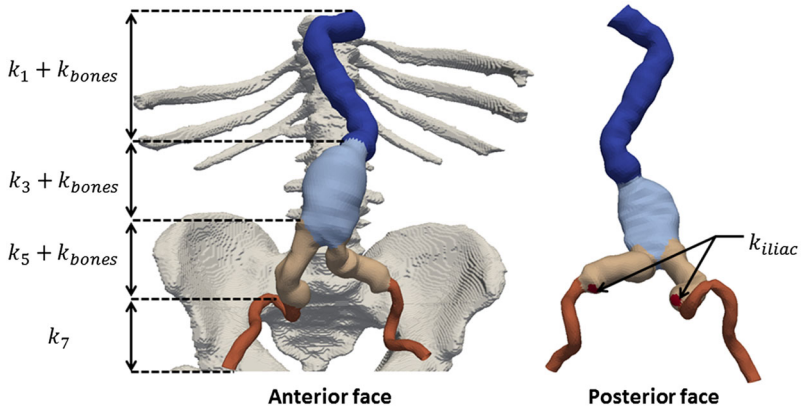


Figure 3. Distribution of elastic support stiffness coefficients along the vascular segments.

### 2.5. *Prestress due to the arterial pressure*

In the context of quasi-static calculations such as those performed in this study, the main effect of the blood pressure is a biaxial pretension of the arterial wall. This prestress affects the tangent stiffness of the arterial wall to a non-negligible degree, and to omit it would lead to a drastic underestimation of the stiffness of the wall *in vivo*. Even though in reality the arterial pressure is variable and cyclic, it can be approximated quite well by a uniform static pressure whose average value is usually set at one-third of the systolic pressure plus two-thirds of the diastolic pressure [4, 21]. Finally, the pressure applied to the internal surface of the mesh is the difference between the internal pressure due to the blood pressure and the external pressure which corresponds to the term $p$ of Equation (2), that is, 0.01 MPa (75 mmHg).

*2.5.1. Modeling of the tools.* The devices which were modeled in our simulations were two Radiofocus Glidecath flexible catheters (Terumo, Somerset, New Jersey, USA) and two Lunderquist 'extra-stiff' guidewires (Cook, Bloomington, Indiana, USA ). The formers generate very little deformation to the arteries, and their goal is to facilitate the insertion of the 'extra-stiff' guidewires used as supports for the stent graft delivery system. We used the real geometry and material properties of extra-stiff guidewires Lunderquist® Cook, which are 0.89-mm diameter stainless steel guidewires. They were modeled using 189 4-mm-long two-noded beam elements with linear elastic properties (Young's modulus $E = 180$ GPa, Poisson's ratio $\upsilon = 0.3$), which are standard values for extra-stiff guidewires [9]. In order to facilitate their insertion, their upper extremities presented a linearly graded elastic modulus from 10 to 180 GPa over a 12-cm length. We did not characterize the mechanical behavior of the soft catheters as they provide negligible stiffness in comparison with the extra-stiff guidewires, their goal being only to ease the introduction of the extra-stiff guidewires. Yet their geometry and material properties were chosen close to those of Radiofocus Glidecath® flexible catheters, with a length of 80 cm, internal diameter of 1.1 mm and thickness 0.6 mm. They were modeled using 2832 qa4 shell elements and material properties similar to those of standard polyurethane plastic (linear elastic material, Young's modulus $E = 1$ GPa, Poisson's ratio $\upsilon = 0.4$).

*2.5.2. Simulation process.* The simulations were performed using the ANSYS LS-DYNA Explicit 15.0 (Ansys, Canonsburg, Pennsylvania, USA) finite element solver on a Dell Precision T7600 workstation equipped with one 8-core Intel-Xeon E5-2687w (3.4 GHz) processor. The simulation process is a two-step process. The first step consists in prestressing the vascular structure by applying the arterial pressure; the second step corresponds to the simulation of the insertion of the endovascular tools.

a. **Application of the prestress due to the arterial pressure**

The reconstructed geometry based on the CT-scan data corresponds to the state of the vascular structure prestressed by several loadings to which it is subjected *in vivo*, including particularly the arterial pressure. Several authors have already described various methods to take into account



DOI: 10.1002/cnm

the prestress induced by the arterial pressure in abdominal aneurysms [21–24]. In our work, we used an iterative method similar to the one described by Bols *et al.* [25] and Riveros *et al.* [26] to determine a new geometry, which corresponds to a stress-free state often called 'zero-pressure geometry'. Then, at the start of the simulation, this geometry is subjected to the internal pressure, which enables one to recover the reference geometry as observed on the scan, except that it now incorporates the prestress due to the pressure. This prestress application step is schematized in Figure 1.

b. **Insertion of the tools**

The insertion of the tools is carried out at the distal end of the external iliac arteries. The tools are pushed into the vascular structure by prescribing a velocity at their lower end until they are fully embedded in the vascular structure. In order to prevent buckling of the tools prior to their insertion into the artery, they are inserted through a rigid introduction tube with a 2-mm diameter. The presence of the rigid introductor also allows the accurate positioning of the tools in terms of both the introduction point and the introduction angle. Inside the vascular structure, the tools are free, and frictionless contact is assumed between them and the internal surface of the lumen. Endovascular guidewires and catheters are designed in order to enhance sliding inside the arteries so their coefficients of friction are very low, thus the assumption of frictionless contact seemed reasonable.

c. **The numerical parameters**

The phenomena, which are modeled at the tool insertion stage, are only slightly dynamic: through observation of intraoperative videos at our disposal, we estimated the actual penetration velocities of the devices, catheters, and guidewires during the endovascular procedure to be in the order of 50 to 500 mm/s, which corresponds to actual sequences of about 1 to 15 s. Therefore, in order to achieve reasonable calculation times, the simulations are slightly accelerated by increasing the insertion rate of the tools and using a mass-scaling method to increase the time step of the explicit calculation. Because the guidewires and catheters are the limiting factors in terms of computation time, their density is artificially increased to achieve an initial time step of $5.10^{-6}$ s, then kept constant for the rest of the calculation. The density of the vascular structure is not modified. Finally, in order to limit the vibrations due to the numerical calculations, damping is introduced into the system via two parameters: parameter $c$ defined in Equation (2) for the vascular structure, and a Rayleigh damping proportional to the mass applied to the elements of the catheter. To ensure that the mass and time scaling does not affect the quasi-static nature of the computation, for both the vascular structure and the guidewires, we checked that kinetic energy remains low compared with the internal energy as can be attested by the energies plotted on Figure 4.

### *2.6. Acquisition and processing of the intraoperative data*

*2.6.1. Acquisition of the intraoperative data.* The endovascular procedure took place in the TherA-Image hybrid platform of the University Hospital of Rennes, which is equipped with an Artis Zeego (Siemens, Munich, Germany) rotational system capable of acquiring 2D fluoroscopic images as well as performing cone-beam CT (CBCT) rotational acquisitions allowing the reconstruction of a 3D volume. At the beginning of the procedure, two CBCT acquisitions were carried out. The first acquisition, which corresponds to the undeformed CBCT, was performed on the vascular structure unaffected by the tools at the beginning of the procedure. Then, a flexible catheter followed by a Lunderquist-type rigid guidewire were introduced into each iliac artery up to the level of the aortic arch, generating significant arterial deformations, at which point a second acquisition corresponding to the deformed CBCT was performed. After that, the procedure continued normally according to the standard protocol for this type of intervention, and the 2D angiographic images acquired during the rest of the procedure were also saved so they could be compared qualitatively with the simulation results. Any imaging acquisitions used during this study were part of a routine protocol. No extra acquisitions were performed for the need of the study. Depending on the particularity of each EVAR cases, some acquisitions can be performed or not during the procedure; for this study we specifically chose the patients who underwent 3D rotational acquisitions.



DOI: 10.1002/cnm

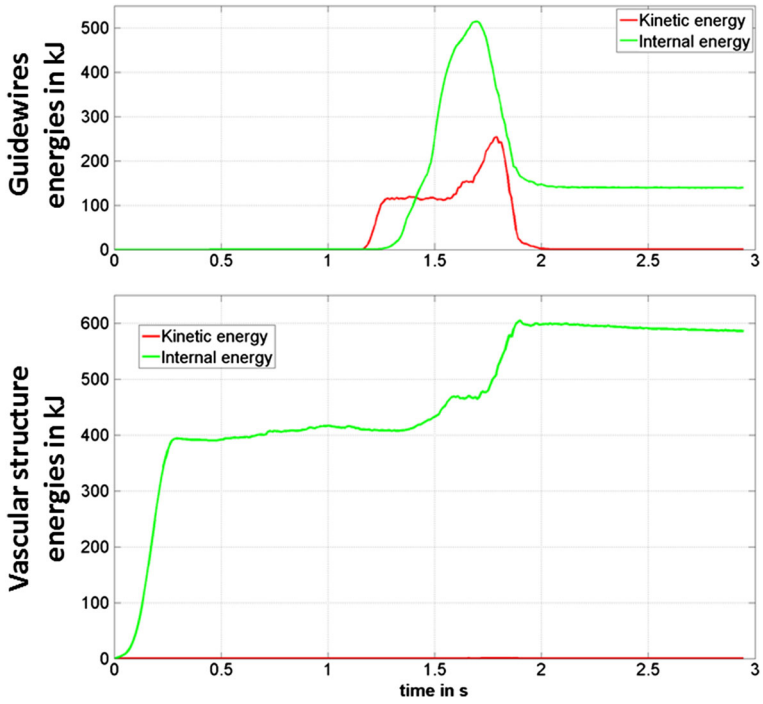


Figure 4. Comparison of kinetic energy and internal energy evolution for the vascular structure and the guidewires.

*2.6.2. Segmentation.* In order to allow their comparison with the simulation results, the structures of interest (i.e., the calcifications enabling the registration and the guidewires enabling the calculation of the simulation error) had to be segmented on the intraoperative images.

Because of their high density, the guidewires are clearly visible on the intraoperative images. They were segmented automatically by thresholding. Then, they were approximated by B-spline curves which were sampled along their curvilinear abscissa starting at their insertion point in order to match a point of the spline with each node of the simulated guidewire.

The calcified plaques, which extended over the common iliac arteries and the abdominal aorta, were located on the undeformed CBCT and on the preoperative CT scan. Their high density compared with the healthy aortic tissue allowed an automatic segmentation by region growth. Then, a two-by-two correspondence of the plaques between the two volumes was established, and the position of the barycenter of each plaque was determined.

*2.6.3. Registration.* Because the CBCT data lie in the intraoperative coordinate system, they must be registered through a rigid 3D/3D transformation in the preoperative coordinate system in order to compare them with the simulation results. In order to do that, the required rigid transformation was determined by matching the positions of the calcifications of the vascular wall observed on the undeformed CBCT with those observed on the preoperative CT scan. Using an iterative closest-point algorithm [27], we calculated the rigid transformation which minimized, point by point, the distance between the barycenters of the calcifications in the CBCT and of the corresponding calcifications in the preoperative CT-scan. This transformation was applied to the deformed CBCT in order to map it onto the preoperative coordinate system.

### *2.7. Comparison of simulation results with intraoperative data*

Having segmented and registered the intraoperative data in the preoperative coordinate system, we were able to measure the simulation error by comparing the positions of the guidewires. Then, this measured error was used to calibrate the parameters of the external support. After that, a sensitivity



DOI: 10.1002/cnm

analysis of this error with regard to variations of those parameters was carried out. Finally, the predictive capability of the simulation is evaluated on a group of nine patients.

*2.7.1. Measurement of the error.* The position of the simulated guidewires was defined as the position of the guidewires' nodes at the end of the simulation. For each of the simulated guidewires, the metric used to measure the distance to the real intraoperative guidewire was the modified Hausdorff distance (MHD) introduced in [28]. Let us define the distance between two points $p_1$ and $p_2$ as the Euclidean distance $d(p_1,p_2)=\|p_1-p_2\|$. Then the distance between a point $p$ and a set of points $S$ is commonly defined as $d(p_1,S)=\min_{p_2\in S}d(p_1,p_2)$. Finally, let us denote the function that computes the arithmetic mean of a variable $v$ inside a set of points $S=\{p_1,p_2,\ldots,p_N\}$ by $\text{mean}_{p\in S}v(p)=\frac{1}{N}\sum_{i=1}^{N}v(p_i)$, then the MHD between the real guidewire and the simulated guidewire is defined by the Equation (4):

$$d_{\text{MHD}}(S_{\text{real}},S_{\text{simu}})=\max\left(\text{mean}_{p\in S_{\text{real}}}d(p,S_{\text{simu}}),\text{mean}_{p\in S_{\text{simu}}}d(p,S_{\text{real}})\right) \tag{4}$$

This comparison of the positions of the simulated guidewires with their intraoperative counterparts is illustrated in the example of Figure 9.

*2.7.2. Calibration of the model.* The model's parameters were tuned manually by trial and error in order to reduce the simulation error defined for each guidewire by the MHD to the real intraoperative guidewire. The calibration was considered to be acceptable once the error for each guidewire became less than 3 mm, which corresponds to the error level obtained by projecting the results of simulations performed by Dumenil *et al.* [11] onto 2D projection images (2.8 mm average). The set of parameters obtained after this calibration phase is called the 'nominal configuration'.

*2.7.3. Sensitivity estimation.* The procedure we used consists in allowing one parameter at a time to vary with respect to the nominal configuration. We studied the evolution of the mean simulation error for the two guidewires as a function of these variations. This method cannot completely describe the space of variation of the parameters, but it gives an idea of the relative influence of each parameter near the nominal configuration and is the first step towards a more thorough sensitivity analysis or parameters optimization. We studied the effect of the external support parameters $\{k_1, k_3, k_5, k_7, d_{\max}\}$.

Because very little information is available in the literature concerning this kind of parameters, parameters $\{k_1,k_3,k_5,k_7\}$ (which correspond to the healthy aorta, the aneurysmal aorta, the common iliac arteries, and the iliac arteries, respectively) were tested individually between a very small value corresponding to no support and a high value corresponding to a totally fixed condition. The parameter $d_{\max}$, which defines the distance of influence of the bones support (Equation (3)), was tested between 0 to 150 mm, 0 corresponding to no bones support. Table I summarizes the parameters which were tested in our study and their ranges of variation.

*2.7.4. Predictive capability evaluation.* Once the set of parameters has been found from the calibration phase, we evaluated the predictive capability of the simulation on a group of nine patients. The overall procedure was exactly the same (3D data acquisition during EVAR procedure, finite element modeling, simulation steps), except that only one catheter and one extra-stiff guidewire were introduced. For all these nine cases, the same parameters (determined from the calibration phase of the first case) were used, and no further calibration was conducted. Like for the calibration patient, the MHD was used to measure the error in the guidewire final position predicted by the simulation. In accordance with surgeons, the simulation prediction is considered acceptable when the MHD between the simulated and the real guidewire is less than 3 mm.



DOI: 10.1002/cnm

Table I. Summary of the values of the parameters tested for sensitivity study.

| Parameter | Nominal value | Minimum | Maximum |
|---|---|---|---|
| $k_1$ | 0.0002 MPa/mm | Free | Fixed |
| $k_3$ | 0.0002 MPa/mm | Free | Fixed |
| $k_5$ | 0.0001 MPa/mm | Free | Fixed |
| $k_7$ | 0.00001 MPa/mm | Free | Fixed |
| $d_{max}$ | 20 mm | 0 mm | 150 mm |

## 3. RESULTS

### 3.1. Calibration phase

*3.1.1. Registration error.* The registration error between the preoperative CT scan and the approximate reference geometry (Figure 1) was measured at nine points which correspond to the barycenters of the calcified plaques. The point-to-point error, the average error per arterial segment, and the global average error are reported in Table II.

*3.1.2. Mesh convergence.* First and foremost, a sensitivity study of the mesh discretization was carried out in order to assess mesh convergence. The evolution of the simulation error with the number of mesh nodes is presented Figure 5 and shows that the convergence of the mesh is achieved for a number of nodes greater than about 8500.

*3.1.3. Simulation error.* The iterative phase of determination of the zero-pressure geometry took approximately 3 h (about 25 7-min iterations), and the calculation of the tool insertion phase took approximately 2.5 h. After the calibration phase, the errors in the guidewires position measured with the MHD were 2.26 mm for the left-hand guidewire and 1.93 mm for the right-hand guidewire. The resulting mean simulation error is calculated as the average of these two values and equals to 2.1 mm. These errors include both the registration error and the simulation error.

Table II. Registration error calculated at calcifications barycenters and average error for the common iliac arteries segment, the aorta segment, and global mean registration error.

| (in mm) | Common iliac arteries | | | | Aorta | | | | |
|---|---|---|---|---|---|---|---|---|---|
| Point-to-point error | 3.38 | 1.74 | 1.79 | 1.04 | 2.16 | 1.98 | 2.08 | 1.79 | 3.18 |
| Segment average | 1.99 | | | | 2.24 | | | | |
| Global average | 2.13 | | | | | | | | |

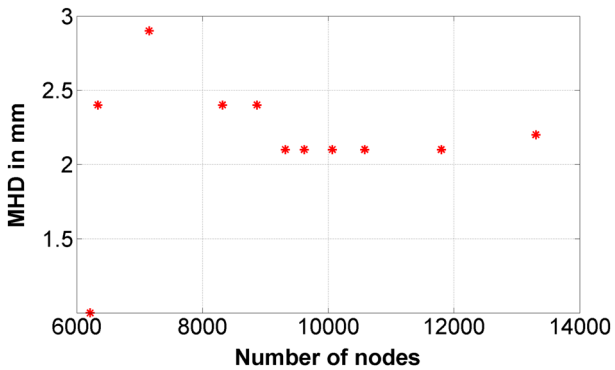


Figure 5. Evolution of simulation error with mesh discretization. MHD, modified Hausdorff distance.



DOI: 10.1002/cnm

### 3.2. *Sensitivity estimation*

Figures 6, 7, and 8 show the evolution of the average MHD in the left and right guidewires as a function of the support stiffness parameters and $d_{max}$. Beyond 3 mm, the error is considered unacceptable for targeted clinical applications.

For the extreme values of $k_1$ and $k_3$, the error in the guidewires remains below 3 mm. However, the error is more sensitive to variations of parameters $k_5$ and $k_7$. It goes up to 3.4 mm for values of $k_5$ inferior to the nominal value and up to 5.4 mm in the case where the common iliac segments were fixed. Regarding $k_7$, one observes a small variation between the free state and a value of

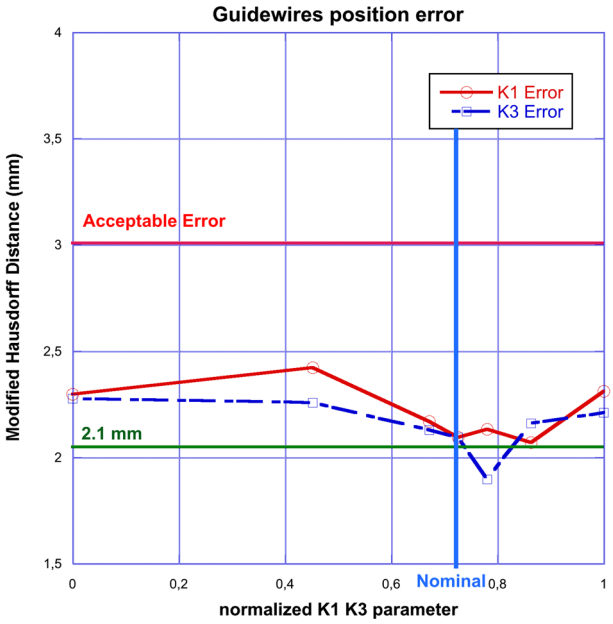


Figure 6. Evolution of simulation error as a function of values of stiffness of external supports $k_1$ and $k_3$.

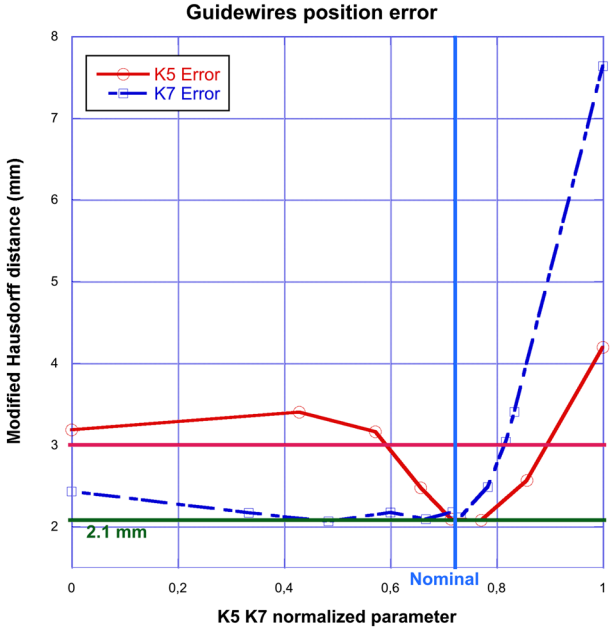


Figure 7. Evolution of simulation error as a function of values of stiffness of external supports $k_5$, and $k_7$.



DOI: 10.1002/cnm

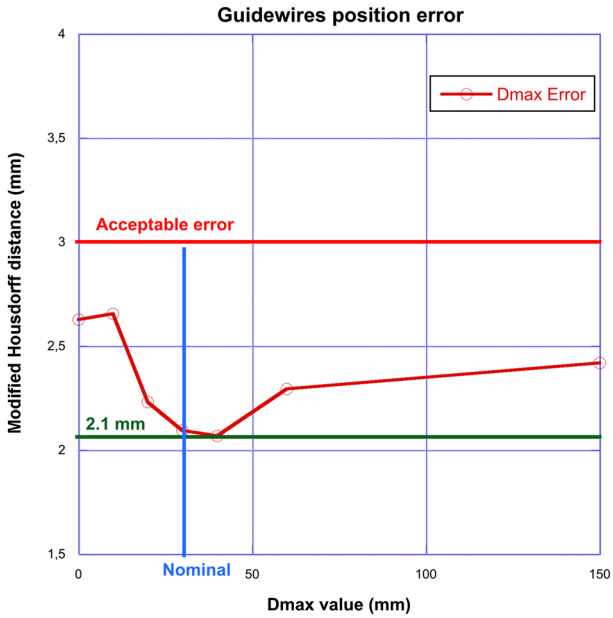


Figure 8. Evolution of simulation error as a function of values of dmax.

approximately 0.0001 MPa/mm which corresponds to the nominal value. Beyond that, the error rises sharply and reaches 16.3 mm when the external iliac segments are fixed. Concerning $d_{\max}$, the error goes up for low values corresponding to weaker and less extended bone support but remains below 3 mm, the error also rises up with increased values of $d_{\max}$ but remains moderate.

### *3.3. Predictive capability evaluation*

For nine other patients, the same simulation process was conducted for the insertion of only one catheter and one extra-stiff guidewire. The simulation ran without problem for the nine patient cases, even for those presenting the most tortuous or calcified anatomies. For each patient, the final guidewire position was compared with the real 3D position of the intraoperative guidewire, and the MHD was measured. The results are summed up in Table III; they encompass both the registration and the simulation error. For four patients, the simulation was able to predict the guidewire position with an error inferior to 3 mm. The mean MHD to the real guidewire and standard deviation were $4.6 \pm 2.5$ mm. Final deformed vascular structure and comparison between simulated guidewire and real operative guidewire positions are illustrated on the calibration case and three of the evaluation cases Figure 9.

Table III. Modified Hausdorff distance (MHD) between simulated guidewire and real intraoperative guidewire on nine evaluation patient cases.

| Patient ID | MHD (mm) |
|---|---|
| 1 | 2.65 |
| 2 | 1.90 |
| 3 | 7.78 |
| 4 | 9.11 |
| 5 | 2.79 |
| 6 | 5.46 |
| 7 | 3.83 |
| 8 | 5.35 |
| 9 | 2.33 |
| Mean | 4.6±2.5 |



DOI: 10.1002/cnm

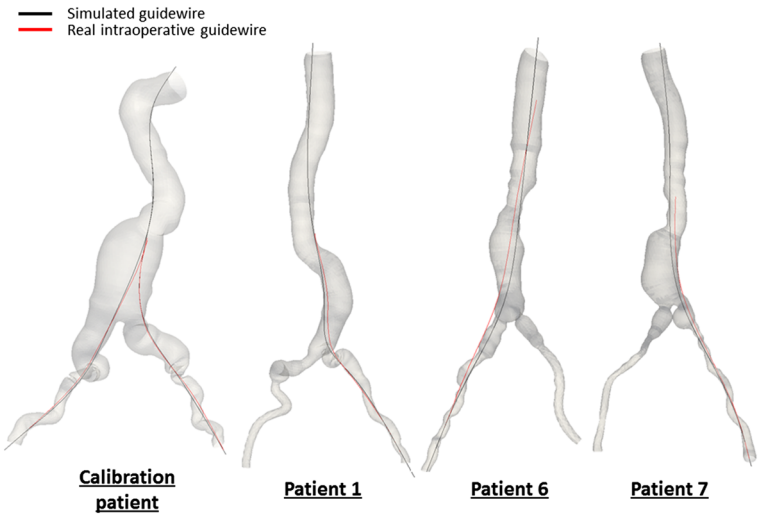


Figure 9. Illustration of deformed vascular structure and guidewire position compared with real intraoperative guidewire on calibration patient and three evaluation patient cases.

## 4. DISCUSSION

### *4.1. Results*

We present the construction of a patient-specific mechanical model of the aorto-iliac vascular structure of a patient and a simulation method for the insertion of flexible endovascular catheters, then extra-stiff guidewires, using an explicit finite element method. We were able to compare the simulation results with the corresponding 3D intraoperative data. The mechanical model takes into account the support brought about by the external environment of the vascular structure. We determined reasonable ranges of variation for the parameters that were introduced to model this external support, as very few experimental or clinical data are available in the literature.

On the patient-specific case used for the calibration and the sensitivity study, we found that the model could be easily tuned to match the intraoperative observations. An average 2.1 mm error in the position of the guidewires seems reasonable for the purpose of predicting the global deformations of the vascular structure in order to assist in the preoperative sizing or to facilitate the intraoperative steering. A sensitivity analysis of the final position of the guidewires with respect to the external support parameters showed the significant influence of the stiffness in the zone which corresponds to the common iliac arteries ($k_5$) and the importance of characterizing this stiffness with great accuracy, in the order of ±0.001 MPa/mm, in order to obtain relevant results. As for the stiffness of the support in the zone, which corresponds to the external iliac arteries (parameter $k_7$), it must remain small in order to avoid overstiffening the external iliac segments. The measured simulation error varies moderately with respect to parameter $d_{\max}$, which drives the stiffness and the extent of bones support; however, we can clearly see that this error tends to go up when the bones support is weakened and, respectively, the model becomes overly stiff when the bones support is extended to a distance higher than approximately 50 mm. Finally, parameters $k_1$ and $k_3$, which correspond to the aortic segments, seem to have little influence on the results. For parameter $k_1$, this can probably be explained by the fact that at the level of the abdominal aorta the vascular structure is already firmly held against the spine by support condition (3), so the lesser additional support brought about by parameter $k_1$ on the posterior side of the aorta seems comparatively negligible. The limited influence of parameter $k_3$ could be explained by the fact that, in this particular case, the guidewires have minimal contact with the vascular structure in the vicinity of the aneurysm, and therefore, the deformations are hardly affected by the support parameter in this zone. Also, the apparent low influence of parameters corresponding to the upper part of the aorta $k_1$ and $d_{max}$ has to be balanced by the fact that the image of the real guidewire is only visible up to the aortic neck, as a result, even if we can suppose that these parameters have a potential influence on the



DOI: 10.1002/cnm

upper part of the guidewire final position, this cannot be measured on this specific case. In any case, it would be necessary to verify these phenomena in other patient-specific cases prior to making definitive statements on the relative influence of the various parameters.

Overall, the limited sensitivity of the model to relatively broad ranges of variation of the parameters shows that the deformation caused by the guidewires depends, first and foremost, on intrinsic properties of the anatomy of the vascular structure, especially its tortuousness and its relation to bones structures.

The simulation process was then evaluated on a group of nine patients with the parameters values found from the calibration phase. Even if the calibration of the parameters was done on one patient-specific case only, the simulation was able to predict the final position of the extra-stiff guidewire for four cases within 3-mm error, and for all cases, the average simulation error was $4.6 \pm 2.5$ mm. These relatively good results show the versatility of the model, yet the prediction performance can be improved by a parameter calibration conducted on a larger number of patient cases.

### *4.2. Relation to previous published data*

The work presented in this paper is a follow-up of previously published studies by our group [11, 10]. Compared with them, it focuses more thoroughly on the mechanical modeling of the vascular structure and the external support, as well as the finite element method used to model endovascular devices introduction. It also presents a new comparison method based on 3D intraoperative data, which improve the model validation and make the results more reliable. More specifically,

- The mechanical modeling of the wall has been improved by the use of a nonlinear hyperelastic model and the incorporation of blood pressure pretension;
- The external environment support has been modeled in a more realistic and versatile manner in order to study the effect of the introduced empirical parameters; and
- The simulation process was improve by using a more realistic process for the tools introduction in association with an explicit finite-element solver in order to reach robustness against all kind of anatomies, particularly the most tortuous ones, which was not the case with the previous method.

Yet the drawback of the increased complexity of the model along with the use of an explicit solver is necessarily longer computation times.

### *4.3. Limitations*

The presence of a significant intraluminal thrombus in the patient case used for calibration and sensitivity study was not taken into account in the model. Nevertheless, because the deformations of the vascular structure in the aneurysmal zone were very small, one would assume that in this particular case, the presence of the thrombus would have had only limited influence on the results.

The material model used was of the hyperelastic polynomial isotropic potential type. One should note that the behavior obtained using such a model is globally 'less stiffening' than that observed in the characterizations of [14]. An exponential anisotropic model with two or four families of fibers [29, 30] would have led to a better fit with the experimental characterizations, and possibly to better simulation results, but such a model was not directly available in LS-DYNA software for shell elements. Nevertheless, considering the relatively small influence of the material behavior on the results of the simulation, it may be preferable to use a constitutive relation which is less costly in terms of CPU time, which is what we did in this work.

In our model, the vascular structure is represented from the femoral bifurcation up to the level of the aortic hiatus; this corresponds to the part that is visible on the preoperative CT scan. However, during surgery, the extra-stiff guidewires are usually inserted up to the end of the aortic arch, almost touching the aortic valve. The high curvature imposed on the tip of guidewires in the arch is therefore not taken into account in our model, whereas it can have an influence on the results. For one patient for which a thoraco-abdominal CT scan was available, we were able to run the simulation with and without taking into account the aortic arch. The results show that on the upper part of the guidewire, the result are generally closer to reality when the aortic arch is modeled, yet its



DOI: 10.1002/cnm

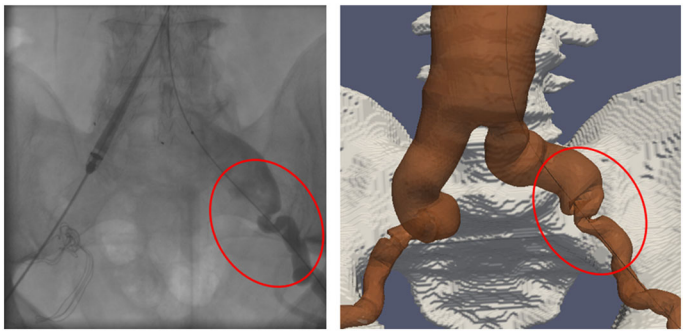

Figure 10. Qualitative comparison between the real intraoperative shape of the vascular structure deformed by guidewires and the deformed shape given by the simulation, highlighting the existence of local buckling of the wall with the formation of folds in both cases.

influence tends to fade away in the lower part of the guidewire and seems negligible in the distal part to the aortic neck. The influence of the presence of the aortic arch in the simulation seems moderated but will have to be further investigated on a larger number of patients. Yet if the interest is only focused on the distal part of the vascular structure, below the aortic neck, it seems reasonable not to take it into account in the simulation.

Some of the results obtained in our various simulations were difficult to interpret and revealed the presence of instabilities in the model behavior. Indeed, we observed the presence of local buckling of the arterial wall with the formation of folds, particularly at the level of the external iliac arteries. These phenomena, which can be the results of numerical bifurcations, can lead to irregularities in the behavior of the model shown, for example, by 'jumps' in the result curves. In order to improve the interpretation, we chose not to use the few results which appeared too irregular. However, these phenomena do correspond to the physical reality because the folds observed in the simulations are also present in the intraoperative images at the level of the external iliac arteries, as shown in Figure 10, and have been previously reported in the literature [31]. Besides, these structural instabilities have relatively little influence on the global behavior of the model because they are usually very localized at the level of the external iliac arteries.

Finally, the model, which was presented in this work, was tested only on a single patient-specific case, but continuing work intends to adjust this model for a representative group of patients in order to arrive at a parameterized patient-specific model.

## 5. CONCLUSION

This work presents a new method to compute the deformation of an aorto-iliac structure induced by endovascular extra-stiff guidewires. The mechanical model takes into account the support due to the external environment of the vascular structure. A sensitivity study helped us characterize the influence of each of the empirical parameters that were introduced to model this support and pinpoint the ones that need to be tuned the most precisely. The simulation results were blindly evaluated against 3D intraoperative data on nine patients. The results show the robustness of the numerical method even for complex tortuous anatomies. Once the predictive capability of the simulation is attested on a larger number of cases, the model will allow us to easily compute clinically relevant data, like arterial segment shrinkage, length of the stent-graft to be deployed, and displacement of important anatomical points like ostia of secondary arteries.

## ACKNOWLEDGEMENTS

This work has been partially conducted in the experimental platform TherA-Image (Rennes, France) supported by Europe FEDER. This work as been partially supported by the French National Research Agency (ANR) in the context of the Endosim project (grant no. ANR-13-TECS-0012).



DOI: 10.1002/cnm

## REFERENCES


1. Dawson DL, Hellinger JC, Terramani TT, Najibi S, Martin LG, Lumsden AB. Iliac artery kinking with endovascular therapies: technical considerations. *Journal of Vascular and Interventional Radiology* 2002; **13**(7):729–733.
2. Maurel B, Hertault A, Gonzalez TM, Sobocinski J, Le Roux M, Delaplace J, Azzaoui R, Midulla M, Haulon S. Evaluation of visceral artery displacement by endograft delivery system insertion. *Journal of Endovascular Therapy* 2014; **21**(2):339–347.
3. Gokani VJ, Fishwick NG, Choke E, Bown MJ, Sayers RD. 'Trial of stiff guidewire': a useful adjunct to determining suitability for endovascular aneurysm repair. *European Journal of Vascular and Endovascular Surgery* 2012; **44**(5):527.
4. Raghavan ML, Vorp DA, Federle MP, Makaroun MS, Webster MW. Wall stress distribution on three-dimensionally reconstructed models of human abdominal aortic aneurysm. *Journal of Vascular Surgery* 2000; **31**(4):760–769.
5. Rodriguez JF, Martufi G, Doblaré M, Finol EA. The effect of material model formulation in the stress analysis of abdominal aortic aneurysms. *Annals of Biomedical Engineering* 2009; **37**(11):2218–2221.
6. Vande Geest JP, Schmidt DE, Sacks MS, Vorp DA. The effects of anisotropy on the stress analyses of patient-specific abdominal aortic aneurysm. *Annals of Biomedical Engineering* 2008; **36**(6):921–932.
7. Auricchio F. Patient-specific aortic endografting simulation from diagnosis to prediction. *Computers in Biology and Medicine* 2013; **43**(4):386–394.
8. Perrin D, Badel P, Avril S, Albertini J-N, Orgeas L, Geindreau C, Duménil A, Goksu C. Patient-specific simulation of stent-graft deployment within an abdominal aortic aneurysm, CMBE Proceedings series, P. Nithiarasu ; R. Löhner ; Kim M. Liew, Hong-Kong, 2013; 367–370.
9. Gupta A, Sett S, Wolf B. Investigation of interaction between guidewire and native vessel using finite element analysis, 2010.
10. Kaladji A, Dumenil A, Castro M, Cardon A, Becquemin J-P, Bou-Saïd B, Lucas A, Haigron P. Prediction of deformations during endovascular aortic aneurysm repair using finite element simulation. *Computerized Medical Imaging and Graphics* 2013; **37**(2):142–149.
11. Dumenil A, Kaladji A, Castro M, Esneault S, Lucas A, Rochette M, Goksu C, Haigron P. Finite-element-based matching of pre- and intraoperative data for image-guided endovascular aneurysm repair. *Biomedical Engineering, IEEE Transactions on* 2013; **60**(5):1353–1362.
12. Mouktadiri G, Bou-Saïd B, Walter-Le-Berre H. Aortic endovascular repair modeling using the finite element method. *Journal of Biomedical Science and Engineering* 2013; **6**(9):917–927.
13. Raghavan ML, Kratzberg J, Castro de Tolosa EM, Hanaoka MM, Walker P, Simao da Silva E. Regional distribution of wall thickness and failure properties of human abdominal aortic aneurysm. *Journal of Biomechanics* 2005; **39**:3010–3016.
14. Vande Geest JP, Sacks MS, Vorp DA. The effects of aneurysm on the biaxial mechanical behavior of human abdominal aorta. *Journal of Biomechanics* 2006; **39**:1324–1334.
15. Schriefl AJ, Zeindlinger G, Pierce DM, Regitnig P, Holzapfel GA. Determination of the layer-specific distributed collagen fibre orientations in human thoracic and abdominal aortas and common iliac arteries. *Journal of the Royal Society Interface* 2011; **9**(71):1275–1286.
16. Chaikof EL, Fillinger MF, Matsumura JS, Rutherford RB, White GH, Blankensteijn JD, Bernhard VM, Harris PL, Kent KC, May J, Veith FJ, Zarins CK. Identifying and grading factors that modify the outcome of endovascular aortic aneurysm repair. *Journal of Vascular Surgery* 2002; **35**(5):1061–1066.
17. Maier A, Gee MW, Reeps C, Eckstein HH, Wall WA. Impact of calcifications on patient-specific wall stress analysis of abdominal aortic aneurysms. *Biomechanics and Modeling in Mechanobiology* 2010; **9**:511–521.
18. Liu Y, Dang C, Garcia M, Gregersen H, Kassab GS. Surrounding tissues affect the passive mechanics of the vessel wall: theory and experiment. *American Journal of Physiology-Heart and Circulatory Physiology* 2007; **293**:3290–3300.
19. Zhang W, Liu Y, Kassab GS. Viscoelasticity reduces the dynamic stresses and strains in the vessel wall: implications for vessel fatigue. *American Journal of Physiology - Heart and Circulatory Physiology* 2007; **293**(4): H2355–H2360.
20. Moireau P, Xiao N, Astorino M, Figueroa CA, Chapelle D, Taylor CA, Gerbeau J-F. External tissue support and fluid–structure simulation in blood flows. *Biomechanics and Modeling in Mechanobiology* 2011; **11**:1–18.
21. De Putter S, Wolters B, Rutten M, Breeuwer M, Gerritsen F, Van De Vosse F. Patient-specific initial wall stress in abdominal aortic aneurysms with a backward incremental method. *Journal of Biomechanics* 2006; **40**(5):1081–1090.
22. Lu J, Zhou X, Raghavan ML. Inverse elastostatic stress analysis in pre-deformed biological structures: demonstration using abdominal aortic aneurysms. *Journal of Biomechanics* 2006; **40**(3):693–696.
23. Raghavan ML, Baoshun M, Fillinger MF. Non-invasive determination of zero-pressure geometry of arterial aneurysms. *Annals of Biomedical Engineering* 2006; **34**(9):1414–1419.
24. Gee M, Reeps C, Eckstein H, Wall W. Prestressing in finite deformation abdominal aortic aneurysm simulation. *Journal of Biomechanics* 2009; **42**(11):1732–1739.
25. Bols J, Degroote J, Trachet B, Verhegghe B, Segers P, Vierendeels J. A computational method to assess the *in vivo* stresses and unloaded configuration of patient-specific blood vessels. *Journal of Computational and Applied Mathematics* 2013; **246**:10–17.
26. Riveros F, Chandra S, Finol E, Gasser TC, Rodriguez J. A pull-back algorithm to determine the unloaded vascular geometry in anisotropic hyperelastic AAA passive mechanics. *Annals of Biomedical Engineering* 2013; **41**(4):694–708.
27. Besl PJ, McKay ND. A method for registration of 3-D shapes. *Pattern Analysis and Machine Intelligence, IEEE Transactions on* 1992; **14**(2):239–256.

28. Dubuisson M-P, Jain AK. A modified Hausdorff distance for object matching, Pattern Recognition, 1994. Vol. 1 - Conference A: Computer Vision & Image Processing., Proceedings of the 12th IAPR International Conference on, **1**, 1994; 566–568 vol.1.
29. Ferruzzi J, Vorp DA, Humphrey JD. On constitutive descriptors of the biaxial mechanical behaviour of human abdominal aorta and aneurysms. *Journal of the Royal Society Interface* 2010; **8**:435–450.
30. Roccabianca S, Figueroa CA, Tellides G, Humphrey JD. Quantification of regional differences in aortic stiffness in the aging human. *Journal of the Mechanical Behavior of Biomedical Materials* 2013; **29**:618–634.
31. Quinn SF, Kim J, Sheley RC, Frankhouse JH. 'Accordion' deformity of a tortuous external iliac artery after stent-graft placement. *Journal of Endovascular Therapy* 2001; **8**(1):93–98.

## SUPPORTING INFORMATION

Additional supporting information may be found in the online version of this article at the publisher's website.



DOI: 10.1002/cnm